Plaque Morphologic Quantification Reliability of 3D Whole-Brain Vessel Wall Imaging in Patients with Intracranial Atherosclerotic Disease: A Comparison with Conventional 3D Targeted Vessel Wall Imaging

Na Zhang, PhD[1], **Xinfeng Liu, MS**[2], **Jiayu Xiao, MD**[1], **Shlee S. Song, MD**[3], **Zhaoyang Fan, PhD**[1,4,5,*]

[1]Biomedical Imaging Research Institute, Cedars-Sinai Medical Center, Los Angeles, CA, USA.

[2]Department of Radiology, Guizhou Provincial People's Hospital, Guiyang, China.

[3]Department of Neurology, Cedars-Sinai Medical Center, Los Angeles, CA, USA.

[4]Department of Radiology, Keck School of Medicine, University of Southern California, Los Angeles, CA, USA.

[5]Department of Radiation Oncology, Keck School of Medicine, University of Southern California, Los Angeles, CA, USA.

Abstract

Background: 3D whole-brain vessel wall imaging (VWI) has demonstrated exquisite image quality for delineating intracranial atherosclerotic disease (ICAD) and reliability for quantifying normal vessel dimensions. However, its reliability in quantifying plaque morphology remains unknown.

Purpose: To evaluate the plaque morphologic quantification reliability of 3D whole-brain VWI in patients via comparison with 3D targeted VWI and 2D turbo spin-echo (TSE).

Study Type: Prospective.

Population: Thirty-three patients with symptomatic ICAD.

Field Strength/Sequence: 3D and 2D TSE acquired at 3.0T.

Assessment: Each participant underwent two VWI sessions with an interval of 7 to 10 days. Three readers identified in consensus all the plaques on both whole-brain and targeted 3D VWI. Their lumen and vessel wall area and volume, plaque burden, percent stenosis, and vessel wall remodeling were measured for by two independent readers. At each culprit plaque determined by a radiologist, the lumen and vessel wall area, plaque burden, plaque-to-wall contrast ratio (CR), and plaque enhancement ratio (ER) were measured for 2D and 3D VWI methods.

Statistical Tests: Intra-class correlation coefficient (ICC) was used to evaluate for 3D VWI's inter-/intra-observer agreement, inter-scan repeatability, and agreement with 2D TSE in each

---

*Corresponding Author:** Zhaoyang Fan, PhD, 2250 Alcazar Street, Room 104, Los Angeles, CA 90033, Telephone: 310-425-9814, zhaoyang.fan@med.usc.edu.

plaque morphologic measurements. Paired t-test was performed for detecting the differences in plaque-to-wall CR and plaque ER between the two 3D methods.

Results: Eighty-four plaques were detected by both 3D VWI methods. Whole-brain VWI provided excellent inter-/intra-observer agreement (ICCs: 0.79-0.99/0.95-0.99), inter-scan repeatability (ICCs: 0.85-0.99), agreement with 2D TSE (ICC: 0.80-0.94) in all morphologic measurements. ICCs of whole-brain VWI (0.79-0.99) were higher or equal to those of targeted VWI (0.76-0.99). The plaque-to-wall CR and plaque ER were significantly higher on whole-brain VWI than on targeted VWI.

Data Conclusion: 3D Whole-brain VWI provides excellent inter-/intra-observer agreement, inter-scan repeatability, and agreement with 2D TSE in plaque morphologic quantification of ICAD and outperforms 3D targeted VWI.

INTRODUCTION

Intracranial atherosclerotic disease (ICAD) is a major cause of ischemic stroke worldwide (1,2). Despite aggressive medical management, symptomatic ICAD has a poor prognosis with a stroke recurrence rate as high as 13% in the first year (3). To risk-stratify patients with ICAD, traditional imaging methods, including transcranial doppler, CT angiography (CTA), MR angiography (MRA), and digital subtraction angiography, focus on the degree of luminal stenosis. However, this measurement alone is not a reliable indicator of disease severity (4-8).

MR vessel wall imaging (VWI) has demonstrated the potential to identify ICAD lesions and characterize their geometrical and signal intensity features that are associated with recent ischemic cerebrovascular events (9-15). Over the last decade, intracranial VWI has evolved from 2D to 3D acquisition techniques (11). 3D variable-flip-angle turbo spin-echo (TSE) with a thin, oblique imaging slab is a commonly used technique and has been shown to be reliable in quantifying vessel wall morphology of ICAD (16-18). However, such a targeted VWI approach only covers major intracranial arteries with a limited imaging volume and necessitates a relatively long echo time, because of slab-selective excitation, thus resulting in compromised T1 weighting and signal-to-noise ratio (SNR). Recently, whole-brain VWI, which incorporates non-selective excitation and a trailing magnetization flip-down module with 3D variable-flip-angle TSE, was developed to allow large spatial coverage, improved cerebrospinal fluid (CSF) suppression, and enhanced T1 weighting without a considerable sacrifice in scan time (19,20). This technique has been shown to be highly reliable in quantification of intracranial vessel dimensions in healthy volunteers (21). However, for widespread adoption of the technique in clinical practice, there is a need to establish its reliability performance in patient populations.

Thus the aim of this study was to evaluate the plaque morphologic quantification reliability of 3D whole-brain VWI in a symptomatic ICAD patient cohort and conduct a comparison with conventional 3D targeted VWI using 2D TSE VWI as an MR imaging reference.

MATERIALS AND METHODS

Subjects

Institutional review board approval was obtained for this Health Insurance Portability and Accountability Act compliant study, and all participants provided written informed consent prior to imaging. From January 2018 through August 2019, patients from stroke clinic were prospectively recruited if they had a) intracranial stenosis of at least 50% in a large intracranial artery on CTA or MRA, b) history of an ischemic stroke in the distribution of the narrowed vessel confirmed by diffusion weighted imaging, and c) at least one atherosclerotic risk factor (e.g. hypertension, hyperlipidemia, diabetes mellitus, and cigarette smoking). Exclusion criteria included: a) contraindications to MR and gadolinium-based contrast agents, b) coexistent ipsilateral extracranial carotid artery stenosis of at least 50%, c) nonatherosclerosis vasculopathy (e.g. dissection, vasculitis, or Moyamoya disease) or evidence of cardioembolism, and d) history of transluminal intervention.

Imaging protocol

The protocol consisted of two VWI sessions with an interval of 7 to 10 days on a 3T MR system (MAGNETOM Trio, Siemens Healthcare, Erlangen, Germany) equipped with a 32-channel phased array head coil. In each session, the following scans were performed: (a) pre-contrast T1-weighted VWI, including 3D whole-brain VWI, 3D targeted VWI, and single-slice 2D TSE VWI, (b) contrast-enhanced MRA (CE-MRA), and (c) post-contrast T1-weighted VWI, including one 3D VWI sequence (e.g. randomly selected whole-brain VWI in session 1 and targeted VWI in session 2) and 2D TSE. When any of these scans exhibited motion-related image artifacts at the discretion of the MR technologist, reacquisition was allowed. CE-MRA was carried out during intravenous injection of gadodiamide (Omniscan, GE Healthcare, United States) at a dose of 0.1 mmol/kg body weight and an injection rate of 1 mL/sec followed by 20 mL of saline flush. Post-contrast 3D VWI was initiated 2 minutes after contrast administration and immediately followed by a post-contrast 2D TSE VWI scan. A flow chart describing the imaging protocol is shown in Figure 1.

Imaging parameters for the three VWI sequences are summarized in Table 1. To ensure a fair comparison, a group of imaging parameters were matched between the two 3D VWI sequences: resolution = $0.53\times0.53\times0.53$ mm^3, parallel imaging GRAPPA factor = 2, receiver bandwidth = 446 Hz/pixel, echo spacing = 4.92 ms, repetition time = 900 ms. 3D whole-brain VWI was performed with a sagittal imaging volume to cover the head except for the ears and nose (19). 3D targeted VWI was performed with a double-oblique coronal imaging volume prescribed based on low-resolution time-of-flight MRA maximum-intensity-projection images in order to cover the major intracranial arteries (17). 2D TSE was acquired at the probable culprit lesion that was identified by a radiologist (**, 10 years of experience) as the most severe stenosis located in the vessel segment whose

territory accounted for the ischemic event. Slice prescription was performed based on the immediately preceding 3D VWI scan from which the MR technologist reconstructed 3 contiguous 2-mm-thick short-axis slices from this lesion and its adjacent normal vessel segment, respectively, using the multi-planar reconstruction (MPR). Single-slice 2D TSE was then acquired at each of these slices, which allowed for retrospective selection of the slice that best matched the reformats of 3D scans.

Image analysis

Image from subjects who successfully underwent two VWI sessions were transferred to a workstation (Syngo MultiModality Workplace, Siemens Healthcare, Germany) for analysis. The pre-contrast 3D VWI image sets acquired with the same sequence during the two sessions were co-registered using an image fusion function to account for head repositioning. Three readers (2 radiologists (** and **) and 1 MR scientist (**), >8 years of experience in vessel wall image interpretation) reviewed each 3D sequence's pre-contrast images in consensus to determine the presence of atherosclerotic plaques at the anterior, middle, and posterior cerebral arteries, intracranial internal carotid artery, basilar artery, and vertebral artery. Atherosclerotic plaques were identified as focal or diffuse eccentric vessel wall thickening (22). All detectable plaques were recorded for each vessel segment.

The plaques detected in both 3D whole-brain and targeted VWI were analyzed regardless of the degree of stenosis. For each one, 2 to 20 contiguous cross-sections of 0.53 mm thickness that longitudinally covered the whole plaque and a cross-sectional slice from the normal segment adjacent or contralateral to the plaque were reconstructed by a single reader (**) using MPR for each 3D image set. All reconstructed cross-sectional images were analyzed by two independent readers (**, an MR imaging scientist with more than 8 years of work experience in MR VWI image analysis; **, a radiologist with 10 years of experience) using commercial software (VesselMass, Leiden University Medical Center, Leiden, the Netherlands). Specifically, morphologic measurement was performed for (a) lumen and vessel wall area, (b) lumen and vessel wall volume, (c) plaque burden, (d) percent stenosis, and (e) remodeling ratio. According to a previous study (21), contours of lumen and outer wall boundaries were traced manually along the interfaces between the lumen and wall as well as between the wall and surrounding tissue. Horizontal, vertical, and minimum lumen diameters, mean lumen and vessel wall area, and lumen and vessel wall volume were automatically calculated for each plaque by the software. The plaque burden was calculated as the ratio of vessel wall area to vessel area (i.e., lumen area plus vessel wall area) of the plaque slice with the most stenotic lumen. The percent stenosis and remodeling ratios were calculated with following equations (16):

$$\text{Percent stenosis} = (1 - D_p / D_r) \times 100\,\% \text{ and}$$

$$\text{Remodeling ratio} = OA_p / OA_r$$

where D_p is the minimum lumen diameter of the plaque slices, D_r is the mean value of horizontal and vertical lumen diameters of the reference slice, OA_p is the vessel area of the plaque slice with the most stenotic lumen, and OA_r is the vessel area of the reference slice.

The two independent readers both performed the above measurements on the images from the first imaging session. Two weeks later, one reader (**) repeated the measurements on the data from the first imaging session, and the other reader (**) performed measurements on the images from the second imaging session. Representative images with lumen and outer wall boundaries of whole-brain VWI were shown in Supplementary Figure S1.

For each probable culprit lesion identified during scanning, the raw 2D TSE images and location and thickness matched cross-sectional slices reconstructed from 3D VWI were separately analyzed by a single reader (**). Specifically, at the most stenotic slice, lumen and vessel wall area, and plaque burden were determined on pre-contrast images using the method described above. Lesion-to-wall contrast ratio (CR) was determined as the mean signal intensity (SI) of the hyper-intense region of the lesion divided by the mean SI of adjacent normal vessel wall on pre-contrast images. Enhancement ratio (ER) was calculated as the ratio of entire lesion SI to gray matter SI (region-of interest (ROI) was readily prescribed on T1-weighted whole-brain VWI and copied to the images of other sequences) measured on post-contrast images divided by the ratio measured on pre-contrast images. Representative images with ROIs for calculating lesion-to-wall CR and ER were shown in Supplementary Figure S2.

Statistical analysis

Statistical analyses were conducted using SPSS (version 25.0, IBM SPSS Statistics, Armonk, NY). Descriptive analyses were performed to describe the distribution of the variables of interest. Quantitative variables are expressed as means ± standard deviations. The intra-class correlation coefficient (ICC) was used to evaluate the 3D sequences' inter- and intra-observer agreement and scan repeatability of each sequence and the agreement between each of the 3D sequences and 2D TSE in plaque dimension quantification. An ICC value of <0.4 was considered poor agreement, a value of 0.4-0.75 was considered good agreement, and a value of 0.75 was considered excellent agreement (23). Paired t-test was performed for detecting the difference in the lesion-to-wall CR and plaque ER between whole-brain VWI and 3D targeted VWI or 2D TSE VWI. A p value < 0.05 was considered to indicate statistical significance.

RESULTS

Nine patients were excluded due to the contraindications to MR and gadolinium-based contrast agents (two patients), coexistent ipsilateral extracranial carotid artery stenosis of at least 50% (two patients), nonatherosclerosis vasculopathy (e.g. dissection, vasculitis, or Moyamoya disease) or evidence of cardioembolism (four patients), and history of transluminal intervention (one patient). A total of thirty-three patients (25 males, 8 female; age 40-69 years, mean 51±8 years) with an ischemic stroke (2-380 days, median 56 days) were recruited to the study. They had the following co-occurring medical conditions: hypertension (61%), hyperlipidemia (70%), diabetes mellitus (30%), and coronary heart

disease (3%). A family history of ICAD was present in 15% of the cohort. Other health risk factors included a history of smoking (61%) and drinking alcohol (42%).

Thirty-one (94%) subjects successfully underwent two VWI sessions (two patients quit the second session). One patient required repeated targeted VWI during the first session, and 4 patients repeated either whole-brain VWI or targeted VWI during the second session due to noticeable motion artifacts. Representative images with motion artifacts and reacquired images without artifacts were shown on Supplementary Figure S3.

A total of 92 plaques were detected on whole-brain VWI in the 31 patients. Eight of them were excluded from analyses because they were missed by targeted VWI due to the limited coverage, including 7 plaques at the posterior cerebral artery and 1 plaque at the basilar artery. Figure 2 illustrates an example where the lesion at the posterior cerebral artery was missed by the targeted VWI sequence. The remaining 84 plaques were located at the middle cerebral artery (54%), intracranial internal carotid artery (17%), basilar artery (9%), or vertebral artery (20%), respectively. The 31 probably culprit lesions were located at the middle cerebral artery (80%), basilar artery (10%), or vertebral artery (10%), respectively.

Figure 3 illustrates image quality for whole-brain and targeted VWI. For whole-brain VWI, all ICCs of inter-observer agreement were 0.79, all ICCs of intra-observer agreement were 0.95, and all ICCs of inter-scan repeatability were 0.85, indicating excellent reliability in morphologic measurements. For targeted VWI, all ICCs were higher or equal to 0.71, 0.84, and 0.80 for inter-observer agreement, intra-observer agreement, and inter-scan repeatability, respectively, indicating good to excellent reliability in morphologic measurements. The ICCs of inter-observer agreement in vessel wall volume, intra-observer agreement in vessel wall area, and lumen and vessel wall volume, and scan repeatability in lumen and vessel wall volume were equal (ICC=0.99) between whole-brain VWI and targeted VWI. The ICCs of other measurements were higher in whole-brain VWI than in targeted VWI. The lumen and vessel wall volume measurements derived from whole-brain VWI were higher than those derived from targeted VWI, but there was no significant difference (p=0.11 and p=0.21, respectively). All morphologic measurements and ICCs with a 95% confidence interval (CI) of each sequence are summarized in Table 2 and Supplementary Table S1.

The morphologic measurements of the 31 probably culprit plaques for 3D and 2D techniques and their agreement are summarized in Table 3. The ICCs of agreement between whole-brain VWI and 2D TSE were 0.91 (0.75-0.97), 0.94 (0.84-0.98), and 0.80 (0.46-0.92) for lumen area, vessel wall area, and plaque burden, respectively. The ICCs of agreement between targeted VWI and 2D TSE were 0.86 (0.40-0.96), 0.93 (0.60-0.98), and 0.68 (0.12-0.88) for lumen area, vessel wall area, and plaque burden, respectively. Notice that whole-brain 3D VWI exhibited higher ICCs than targeted 3D VWI in all the three measurements (0.91 vs. 0.86 for lumen area, 0.94 vs. 0.93 for vessel wall area, and 0.80 vs. 0.68 for plaque burden.

The lesion-to-wall CR of whole-brain VWI was 1.94±0.31, which was significantly higher than that of targeted VWI (1.48±0.18, p<0.05) and that of 2D TSE (1.66±0.20, p<0.05). The plaque ER of whole-brain VWI (1.94±0.57) was slightly higher than that of 2D

TSE (1.70±0.38, p=0.137) and significantly higher than that of targeted VWI (1.54±0.44, p<0.05). Figure 4 displays an example comparison of plaque ER across all sequences for a patient with a severe stenosis of the left vertebral artery.

DISCUSSION

Our results showed high reliability of 3D whole-brain VWI in morphologic quantification of ICAD lesions. For all morphologic measurements, including lumen and vessel wall area and volume, plaque burden, percent stenosis, and remodeling ratio, 3D whole-brain VWI demonstrated excellent intra- and inter-observer agreement and scan repeatability, which appeared advantageous over 3D targeted VWI of this study and previous studies (17,24-26). We attribute this advantage to the following two features of whole-brain VWI: 1) the remarkable attenuation of surrounding CSF signals improved the conspicuity of the outer boundary of vessel wall, thus facilitating manual contouring; and 2) the enhanced SNR due to shortened echo time was in general beneficial for quantitative image analysis.

Assessments of the inter- and intra-rater agreement and scan repeatability of quantitative plaque measurements is crucial for a clinical use of a VWI technique for determining plaque progression and regression. A previous study has reported high morphologic quantification reliability of 3D whole-brain VWI in healthy volunteers and a small number of patients (21). Our results support those findings and showed comparatively better ICCs and confidence intervals for the lumen and vessel wall volume compared to the previous study on healthy subjects (21). This may be due to the thicker vessel wall and larger separation between vessel outer boundary and brain parenchyma in ICAD patients, both of which would aid in manual contouring of the vessel boundaries and reducing partial volume effects.

Our results also showed that lumen and vessel wall volume measurements derived from whole-brain VWI were higher than those derived from targeted VWI. This is most likely due to the fact that the observer tended to identify more slices on either side of the plaque as thickened vessel wall due to the sharper vessel wall-to-CSF contrast in 8 plaques on whole-brain VWI compared to targeted VWI. However, these differences in measurements between the two VWI techniques were not significant.

For the lumen area, vessel wall area, and plaque burden, excellent agreement was observed between 3D whole-brain VWI and 2D TSE, and good to excellent agreement was observed between 3D targeted VWI and 2D TSE. The ICCs were all higher for 3D whole-brain VWI. Therefore, whole-brain VWI is likely more accurate than targeted VWI for quantitative analysis of plaque morphologic features.

Our study demonstrated significantly higher lesion-to-wall CR and plaque ER in whole-brain VWI than in targeted VWI. This signal-level strength is likely a result of improved T1 contrast. Importantly, these two metrics have been commonly used to indicate the presence of intraplaque hemorrhage and inflammation, respectively, and demonstrated clinically relevant (15,22,27-30). Whether the higher measurements obtained by whole-brain VWI can translate into better detection of vulnerable plaques would be an interesting topic in the future.

There was a timing variation between the two 3D VWI sequences, with the sequence conducted later having the likelihood of image degradation due to motion. However, we repeated the scans whenever appreciable motion artifacts were noticed and all the cases that were included in analysis were motion free. Such a measure could help mitigate the influence of the timing issue on image quality, particularly for session 1 in which intra- and inter-observer agreement analyses were performed. Nevertheless, this issue would not impact the inter-scan repeatability analysis or 3D-2D agreement analyses.

Limitations

First, our study is a single center study using only one type of MRI scanner and software for vessel wall analysis. Reliability may vary across different equipment and software vendors, and this was not assessable. Further research is warranted to determine whether the whole-brain VWI MR protocol demonstrates the same strengths in multiple centers or across different scanner and software types. Second, we used a semi-automatic tool for plaque morphologic measurement, which requires formal training of observers in image analysis to achieve accurate quantification of vessel wall and plaque characteristics. Expertise by observers is needed particularly in difficult cases where the boundary delineation between the outer wall and surrounding tissue is unclear. A fully automatic image analysis tool may further increase efficiency and accuracy of quantification for vessel wall and plaque measurements, enabling atherosclerosis detection and monitoring over a larger territory, with more homogeneity in measurements across studies. Finally, the sample size in our study is still relatively small. Future studies including more patients with similar amounts of lesions at individual major intracranial arteries are warranted.

Conclusion

Whole-brain VWI is reliable for morphological assessment of ICAD and is advantageous over targeted VWI. Whole-brain VWI has potential for use in quantifying longitudinal morphologic changes in ICAD, as well as in monitoring therapy and disease progression.

Supplementary Material

Refer to Web version on PubMed Central for supplementary material.

Grant Support:

REFERENCES

1. Hoshino T, Sissani L, Labreuche J, et al. Prevalence of Systemic Atherosclerosis Burdens and Overlapping Stroke Etiologies and Their Associations With Long-term Vascular Prognosis in Stroke With Intracranial Atherosclerotic Disease. Jama Neurology 2018;75(2):203–211. [PubMed: 29279888]

2. Battistella V, Elkind M. Intracranial atherosclerotic disease. European Journal of Neurology 2014;21(7):956–962. [PubMed: 24612339]

3. Derdeyn C, Chimowitz M, Lynn M, et al. Aggressive medical treatment with or without stenting in high-risk patients with intracranial artery stenosis (SAMMPRIS): the final results of a randomised trial. Lancet 2014;383(9914):333–341. [PubMed: 24168957]

4. Wang Y, Zhao X, Liu L, et al. Prevalence and Outcomes of Symptomatic Intracranial Large Artery Stenoses and Occlusions in China The Chinese Intracranial Atherosclerosis (CICAS) Study. Stroke 2014;45(3):663–669. [PubMed: 24481975]

5. Kasner S, Chimowitz M, Lynn M, et al. Predictors of ischemic stroke in the territory of a symptomatic intracranial arterial stenosis. Circulation 2006;113(4):555–563. [PubMed: 16432056]

6. Lin A, Rawal S, Agid R, Mandell D. Cerebrovascular Imaging: Which Test is Best? Neurosurgery 2018;83(1):5–18. [PubMed: 28973579]

7. Gupta A, Gialdini G, Lerario M, et al. Magnetic resonance angiography detection of abnormal carotid artery plaque in patients with cryptogenic stroke. Journal of the American Heart Association 2015;4(6):e002012. [PubMed: 26077590]

8. Leng X, Wong K, Liebeskind D. Evaluating intracranial atherosclerosis rather than intracranial stenosis. Stroke 2014;45(2):645–651. [PubMed: 24399377]

9. Banerjee C, Chimowitz M. Stroke Caused by Atherosclerosis of the Major Intracranial Arteries. Circulation Research 2017;120(3):502–513. [PubMed: 28154100]

10. Bodle J, Feldmann E, Swartz R, Rumboldt Z, Brown T, Turan T. High-Resolution Magnetic Resonance Imaging An Emerging Tool for Evaluating Intracranial Arterial Disease. Stroke 2013;44(1):287–292. [PubMed: 23204050]

11. Mandell D, Mossa-Basha M, Qiao Y, et al. Intracranial Vessel Wall MRI: Principles and Expert Consensus Recommendations of the American Society of Neuroradiology. AJNR Am J Neuroradiol 2017;38(2):218–229. [PubMed: 27469212]

12. Mossa-Basha M, Alexander M, Gaddikeri S, Yuan C, Gandhi D. Vessel wall imaging for intracranial vascular disease evaluation. J Neurointerv Surg 2016;8(11):1154–1159. [PubMed: 26769729]

13. Mossa-Basha M, Hwang W, De Havenon A, et al. Multicontrast high-resolution vessel wall magnetic resonance imaging and its value in differentiating intracranial vasculopathic processes. Stroke 2015;46(6):1567–1573. [PubMed: 25953365]

14. Tomey M, Narula J, Kovacic J. Advances in the Understanding of Plaque Composition and Treatment Options. Journal of the American College of Cardiology 2014;63(16):1604–1616. [PubMed: 24583311]

15. Wu F, Ma Q, Song H, et al. Differential Features of Culprit Intracranial Atherosclerotic Lesions: A Whole-Brain Vessel Wall Imaging Study in Patients With Acute Ischemic Stroke. Journal of the American Heart Association 2018;7(15).

16. Qiao Y, Anwar Z, Intrapiromkul J, et al. Patterns and Implications of Intracranial Arterial Remodeling in Stroke Patients. Stroke 2016;47(2):434-+. [PubMed: 26742795]

17. Qiao Y, Steinman D, Qin Q, et al. Intracranial Arterial Wall Imaging Using Three-Dimensional High Isotropic Resolution Black Blood MRI at 3.0 Tesla. Journal of Magnetic Resonance Imaging 2011;34(1):22–30. [PubMed: 21698704]

18. Zhang L, Zhang N, Wu J, et al. High resolution three dimensional intracranial arterial wall imaging at 3 T using T1 weighted SPACE. Magnetic Resonance Imaging 2015;33(9):1026–1034. [PubMed: 26143482]

19. Fan Z, Yang Q, Deng Z, et al. Whole-Brain Intracranial Vessel Wall Imaging at 3 Tesla Using Cerebrospinal Fluid-Attenuated T1-Weighted 3D Turbo Spin Echo. Magnetic Resonance in Medicine 2017;77(3):1142–1150. [PubMed: 26923198]

20. Yang Q, Deng Z, Bi X, et al. Whole-Brain Vessel Wall MRI: A Parameter Tune-up Solution to Improve the Scan Efficiency of Three-Dimensional Variable Flip-Angle Turbo Spin-Echo. Journal of Magnetic Resonance Imaging 2017;46(3):751–757. [PubMed: 28106936]

21. Zhang N, Zhang F, Deng Z, et al. 3D whole-brain vessel wall cardiovascular magnetic resonance imaging: a study on the reliability in the quantification of intracranial vessel dimensions. Journal of Cardiovascular Magnetic Resonance 2018;20.

22. Qiao Y, Zeiler S, Mirbagheri S, et al. Intracranial plaque enhancement in patients with cerebrovascular events on high-spatial-resolution MR images. Radiology 2014;271(2):534–542. [PubMed: 24475850]

23. Kroner E, Westenberg J, van der Geest R, et al. High field carotid vessel wall imaging: A study on reproducibility. European journal of radiology 2013;82(4):680–685. [PubMed: 23246333]

24. Qiao Y, Guallar E, Suri F, et al. MR Imaging Measures of Intracranial Atherosclerosis in a Population-based Study. Radiology 2016;280(3):860–868. [PubMed: 27022858]

25. Yang W, Huang B, Liu X, Liu H, Li P, Zhu W. Reproducibility of high-resolution MRI for the middle cerebral artery plaque at 3T. European journal of radiology 2014;83(1):e49–55. [PubMed: 24189388]

26. Zhang X, Zhu C, Peng W, et al. Scan-Rescan Reproducibility of High Resolution Magnetic Resonance Imaging of Atherosclerotic Plaque in the Middle Cerebral Artery. PloS one 2015;10(8):e0134913. [PubMed: 26247869]

27. Liu J, Sun J, Balu N, et al. Semiautomatic carotid intraplaque hemorrhage volume measurement using 3D carotid MRI. Journal of magnetic resonance imaging : JMRI 2019;50(4):1055–1062. [PubMed: 30861249]

28. Wu F, Song H, Ma Q, et al. Hyperintense Plaque on Intracranial Vessel Wall Magnetic Resonance Imaging as a Predictor of Artery-to-Artery Embolic Infarction. Stroke 2018;49(4):905–911. [PubMed: 29540606]

29. Wang M, Wu F, Yang Y, et al. Quantitative assessment of symptomatic intracranial atherosclerosis and lenticulostriate arteries in recent stroke patients using whole-brain high-resolution cardiovascular magnetic resonance imaging. Journal of cardiovascular magnetic resonance : official journal of the Society for Cardiovascular Magnetic Resonance 2018;20(1):35. [PubMed: 29880054]

30. Xiao J, Song S, Schlick K, et al. Serial MR Vessel Wall Imaging Reveals Medical Treatment Response of Symptomatic Intracranial Atherosclerotic Plaque. Proc. Intl. Soc. Mag. Reson. Med 28 (2020):1065.
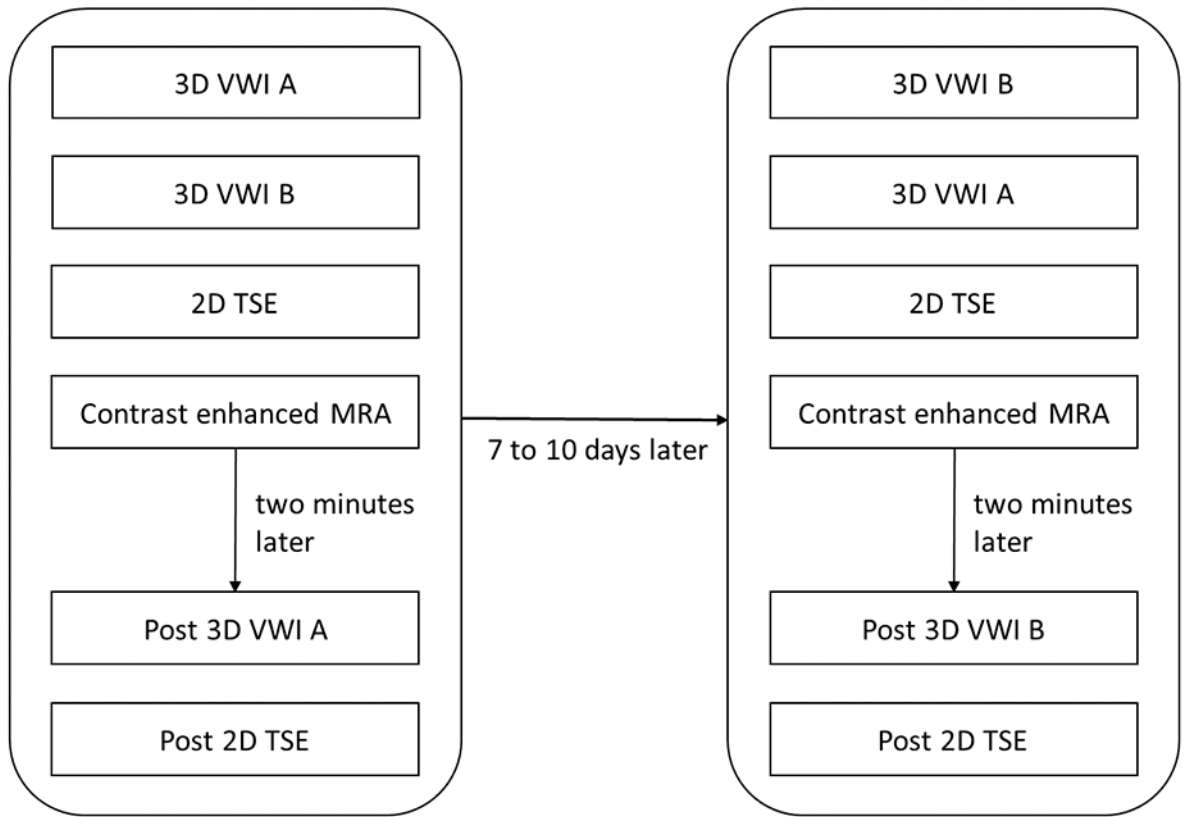
Figure 1.
The flow chart of the imaging protocol. 3D vessel wall imaging (VWI) A was randomly
selected as either whole-brain or targeted VWI; 3D VWI B is the other technique.
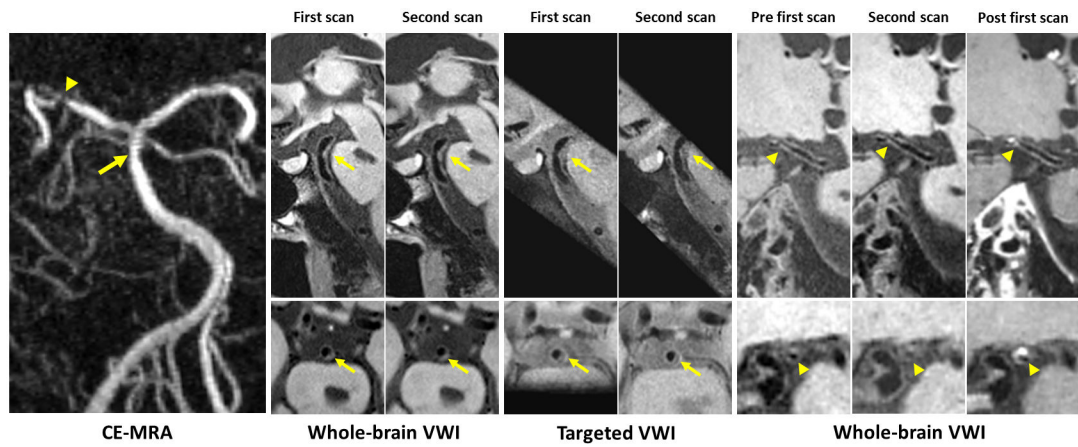
Figure 2.
Representative vessel wall images acquired with 3D whole-brain and targeted vessel wall imaging (VWI) for a patient with a brain stem infarct. Contrast-enhanced magnetic resonance angiography (CE-MRA) shows a slight stenosis of the basilar artery (arrow) and a severe stenosis of the right posterior cerebral artery (arrowhead). All scans of 3D whole-brain and targeted VWI provide good depiction of the two plaques at the corresponding location (arrow and arrowhead) except plaques at the right posterior cerebral artery were missed by targeted VWI due to the limited target coverage. The plaque is considered to be the culprit lesion with obvious enhancement on a post-contrast image.
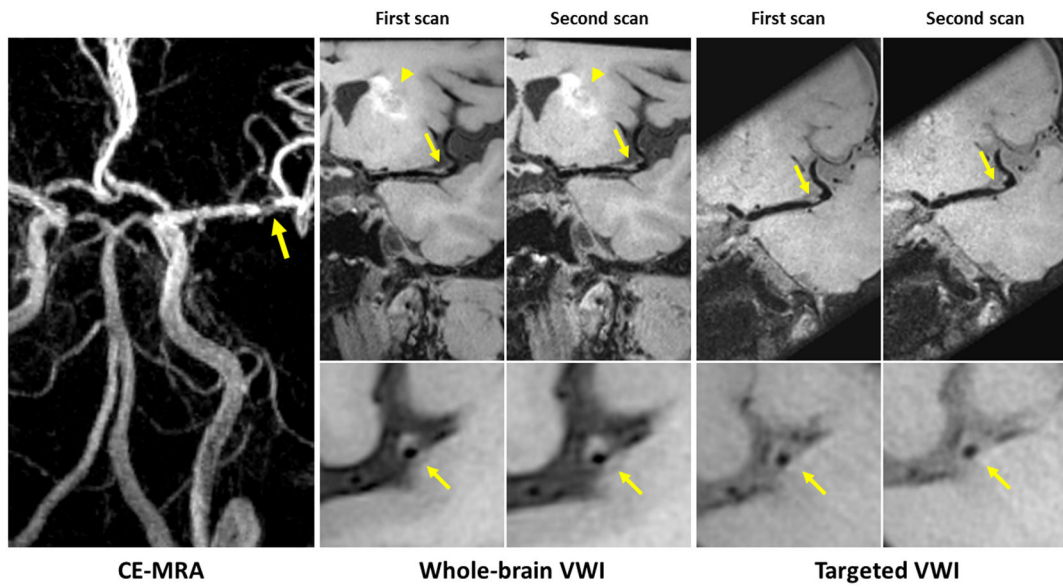
Figure 3.
Representative 3D scan and rescan images of a patient with a left basal ganglia infarct (arrowhead). Contrast-enhanced magnetic resonance angiography (CE-MRA) shows severe stenosis of left middle cerebral artery. Both 3D whole-brain and targeted vessel wall imaging (VWI) depict an eccentric atherosclerotic plaque at the corresponding location (arrows) with good delineation of the plaque on two scans. However, the outer boundary is difficult to assess on the targeted image due to insufficient cerebral spinal fluid (CSF) suppression.
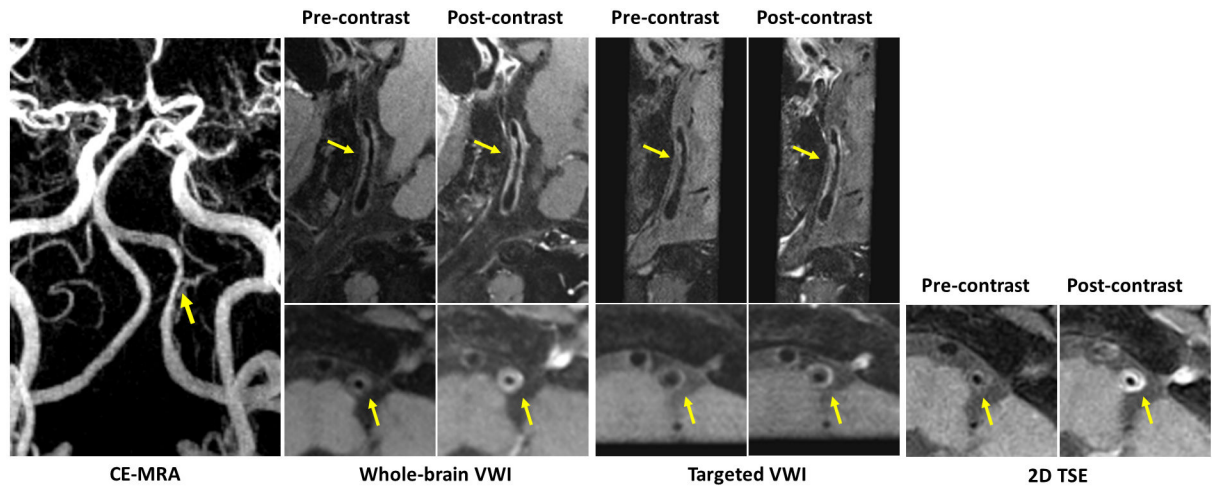
Figure 4.
Representative 3D and 2D images with (post-contrast) and without contrast agent (pre-contrast) for a patient with a severe stenosis of left vertebral artery on contrast-enhanced magnetic resonance angiography (CE-MRA). A long atherosclerotic plaque detected at the corresponding location (arrows) on both 3D whole-brain and targeted vessel wall imaging (VWI) is considered as vulnerable plaque with obvious enhancement on post-contrast images. The post-contrast whole-brain image exhibits similar enhancement of the plaque to the 2D turbo spin echo (TSE) image, but more enhancement than the post-contrast targeted image.

Table 1.

Relevant imaging parameters for the three VWI sequences.

	Whole-brain VWI	Targeted VWI	Single-slice 2D TSE
Resolution (mm^2)	**0.53×0.53**	**0.53×0.53**	0.53×0.53
Slice thickness (mm)	**0.53**	**0.53**	2
Repetition time /echo time (ms)	**900**/15	**900**/30	800/12
Parallel imaging GRAPPA factor	**2**	**2**	N/A
Receiver bandwidth (Hz/Pixel)	**446**	**446**	411
Echo spacing (ms)	**4.92**	**4.92**	11.5
Slice partial Fourier	6/8	Off	N/A
Field of view (mm^3)	170×170×128	170×170×34	136×170
Echo train length	52	26	9
Signal averages	1	2	4
Orientation	Sagittal	Oblique coronal	Cross-sectional
Scan time (min:sec)	8:10	8:3	1:36

Note: Highlighted in bold are the parameters matched between the two 3D VWI sequences. VWI = vessel wall imaging; TSE = turbo spin-echo; GRAPPA = generalized autocalibrating partial parallel acquisition.

Table 2

ICCs with 95% CI of inter- and intra-observer agreement, and scan repeatability in morphologic measurements for each 3D VWI sequence.

ICC (95% CI)		Lumen area	Vessel wall area	Lumen volume	Vessel wall volume	Plaque burden	Percent stenosis	Remodeling ratio
Whole-brain	Inter-observer	0.97 (0.94-0.99)	0.98 (0.94-0.99)	0.99 (0.94-0.99)	0.99 (0.98-0.99)	0.86 (0.71-0.93)	0.88 (0.77-0.94)	0.79 (0.59-0.89)
	Intra-observer	0.99 (0.98-0.99)	0.99 (0.97-0.99)	0.99 (0.99-0.99)	0.99 (0.99-0.99)	0.95 (0.90-0.97)	0.96 (0.92-0.98)	0.95 (0.90-0.97)
	Inter-scan	0.99 (0.98-0.99)	0.99 (0.96-0.99)	0.99 (0.97-0.99)	0.99 (0.99-0.99)	0.90 (0.78-0.95)	0.95 (0.90-0.97)	0.85 (0.72-0.93)
Targeted	Inter-observer	0.81 (0.64-0.90)	0.95 (0.91-0.98)	0.96 (0.93-0.98)	0.99 (0.97-0.99)	0.71 (0.42-0.85)	0.86 (0.71-0.93)	0.76 (0.53-0.88)
	Intra-observer	0.96 (0.93-0.98)	0.99 (0.98-0.99)	0.99 (0.94-0.99)	0.99 (0.98-0.99)	0.84 (0.69-0.92)	0.89 (0.79-0.94)	0.84 (0.69-0.92)
	Inter-scan	0.84 (0.70-0.92)	0.97 (0.94-0.99)	0.99 (0.99-0.99)	0.99 (0.99-0.99)	0.82 (0.62-0.91)	0.94 (0.89-0.97)	0.80 (0.61-0.88)

Note: ICC= intra-class correlation coefficient; CI= confidence interval; VWI=vessel wall imaging.

Table 3

Morphologic measurements and agreement (ICC values with 95% CI) between each of the 3D sequences and 2D TSE.

n=31	3D Whole-brain	2D TSE	ICC (95% CI)	P value (t-test)	3D Targeted	2D TSE	ICC (95% CI)	P value (t-test)
Lumen area (mm^2)	4.40±2.59	4.34±2.22	0.91 (0.75-0.97)	0.85	3.48±1.92	4.40±1.92	0.86 (0.40-0.96)	0.02
Vessel wall area (mm^2)	10.40±7.37	10.38±5.93	0.94 (0.84-0.98)	0.99	7.99±4.45	9.65±5.00	0.93 (0.60-0.98)	0.001
Plaque burden	0.68±0.13	0.70±0.10	0.80 (0.46-0.92)	0.41	0.69±0.08	0.68±0.08	0.68 (0.12-0.88)	0.59

Note: ICC= intra-class correlation coefficient; CI= confidence interval; TSE=turbo spin echo.